International Journal of Mining, Reclamation and Environment

Publication details, including instructions for authors and subscription information:
http://www.tandfonline.com/loi/nsme20

Dragline dynamic modelling for efficient excavation

Nuray Demirel [a] & Samuel Frimpong [b]

[a] Department of Mining Engineering , Middle East Technical University , Ankara, Turkey

[b] Department of Mining and Nuclear Engineering , Missouri University of Science and Technology , MO, USA

Published online: 03 Apr 2009.

To cite this article: Nuray Demirel & Samuel Frimpong (2009) Dragline dynamic modelling for efficient excavation, International Journal of Mining, Reclamation and Environment, 23:1, 4-20, DOI: 10.1080/17480930802091166

To link to this article: http://dx.doi.org/10.1080/17480930802091166

International Journal of Mining, Reclamation and Environment
Vol. 23, No. 1, March 2009, 4–20

Taylor & Francis
Taylor & Francis Group

Dragline dynamic modelling for efficient excavation

Nuray Demirel[a]* and Samuel Frimpong[b]

[a]*Department of Mining Engineering, Middle East Technical University, Ankara, Turkey;*
[b]*Department of Mining and Nuclear Engineering, Missouri University of Science and Technology, MO, USA*

(*Received 31 December 2007; accepted 23 March 2008*)

Overburden excavation is an integral component of the surface mine production chain. In large mines, the walking dragline is a dominant strip mining machine. Production engineers and operators must be guided by appropriate strategies to preserve the structural and operating performance of this equipment to justify its high capital investment. The dragline performance mainly depends on the spatial kinematics and dynamics of its front-end assembly. In this study, the authors developed the dynamic modelling of a dragline front-end assembly incorporating 2-D kinematics and bucket-formation interaction using numerical methods and dynamic simulation environment. Detailed analysis of the simulation results show that the maximum closure error from the model validation function is $4 \times 10\ \mathrm{E}-8$. The angular accelerations of the drag and hoist ropes are close to zero. The respective maximum drag, cutting and hoist forces are 100 kN, 200 kN and 75 kN. The results indicate machine health and longevity within the simulated conditions.

Keywords: dragline; dynamic model; kinematic model; simulation; cutting resistance

1. Introduction

Walking draglines are massive and expensive excavators, which have been extensively used in strip mining operations for overburden removal. Draglines are constructed for heavy-duty cyclic operation. Due to its massive structure and a heavy suspended load, the components of the dragline front-end assembly are under dynamic forces, moments and stresses that arise due to the accelerating inertia in the mechanism. Inefficient dragline operations introduce significant stresses and strains along the boom which may result in additional maintenance costs and could lead to catastrophic structural failure. Also, the lack of knowledge or clear understanding of the main parameters affecting the boom strength and durability may cause mine operators to run the machine below its capacity which could have a negative impact on the overall performance of the dragline. Therefore, production engineers and operators must be guided by appropriate strategies to preserve the operating performance and to ensure the machine longevity in order to justify high capital investment, which ranges between $30 million to $100 million [1,2].

*Corresponding author. Email: ndemirel@metu.edu.tr

ISSN 1748-0930 print/ISSN 1748-0949 online

DOI: 10.1080/17480930802091166
http://www.informaworld.com

The dragline front-end consists of massive and interrelated structures, such as boom, drag, and hoist ropes, and rigging mechanism, which altogether cause the translational and rotational motion in 3-D space. Efficient use of draglines requires a thorough knowledge of the powered functions, the translational and rotational motions and machine-formation interactions within the operating environment.

Kinematics analysis is performed to investigate dragline front-end motion in 2-D space. The vector loop representation is used to characterise the dragline front-end geometry and to provide mathematical expressions for the kinematics model, which explores the relationships between position, velocity and acceleration vectors that capture the 2-D space motions. The simultaneous constraint method is used to build the dynamic model of the front-end assembly to capture the forces, moments and torques incident on the focus areas during excavation. On the basis of the kinematics and dynamic simulations, component stress modelling and analysis could be performed using finite element methods in a mechanical event and system simulation environment to simulate the stress distribution along the dragline boom under different operating performance and field conditions.

2. Background literature

Kinematics and dynamic modelling of excavators has been studied and reported extensively. Work on coordinated control of excavators began in the mid-1980s by Lawrence *et al*. [3]. In this work [3], an excavator end-point is controlled in cylindrical task space coordinates by an operator rotating with the arm and using a single joystick [4]. Bullock *et al*. [5] and Bernold [6] studied the forces between the soil and a tool (bucket) during digging operations and developed static force/torque relations. Khoshzaban *et al*. [7] developed kinematics equations for machine positioning. Several researchers have developed the kinematic equations of positioning for a front-end loader. Hansen [8] presented a generalised dimensional synthesis of planar mechanisms with revolute and translational joints by solving a set of vector loop equations. Haneman *et al*. [9] developed a physical model to determine the reliability of a dragline bucket and rigging performance. Koivo [10] investigated the kinematics of the backhoe and loader construction excavator to provide a basis for achieving automatic computer-controlled operations using homogenous transformation matrices that relate the adjacent coordinate frames. Frimpong and Hu [11] developed kinematic and dynamic models as a basis for hydraulic shovel situation. Frimpong and Chang [12] have advanced the dynamic and kinematic model of a cable shovel using an exponential and Kane's algorithms. The kinematic model for a hydraulic shovel has been developed using transformation matrix method to describe the motion of the machine [12]. Shi and Joseph [13] developed a kinematic and dynamic modelling of a cable shovel crowd arm based on Newton's first and second laws, and they introduced a new curved dipper design concept. Awuah-Offei *et al*. [14] developed innovative kinematic and dynamic simulation modelling of a cable shovel to optimise specific energy consumption in the excavation of oil sands.

Despite these improvements, existing models and the current body of knowledge lack the robust fundamental theories required for comprehensive dragline simulation, reliability and completeness. Therefore, dynamic modelling and simulation of a dragline front-end is still an emerging research frontier.

3. Dragline dynamic modelling

Draglines operate in a dynamic environment that leads to variable loads and stresses on the machine, and thus, the knowledge of dragline dynamics should provide enough information to make appropriate predictions of the outcome of any achievable cycle. Dynamic model is built to capture dynamic forces that arise due to the accelerating inertia in the mechanism to characterise the machine performance. The simultaneous constraint method is used to build the dynamic model of the dragline front-end. The rationale for using the simultaneous constraint method is that the formulation of the mechanism does not require choosing a set of generalised coordinates to describe the system. It provides a more direct solution procedure using differential calculus. In this method, kinematics constraints and Newton–Euler equations are solved in a system of simultaneous linear equations.

3.1. Kinematic modelling

The dragline kinematics model is developed to investigate its front-end spatial motion during the machine operation. The kinematics modelling employs the vector loop method to provide mathematical expressions for the kinematic relationships among the components of the mechanism during its motion. A vector loop is a closed loop of vectors that represents the key parameters in the mechanism, which include the length between joints as well as their orientations. The schematic diagram (Figure 1a) of a dragline front-end has been used to extract the vector loop representation to characterise the front-end assembly as shown in Figure 1b.

From a fundamental theory of geometry, the vector loop closure equation is given by Equation (1).

$$\sum_{i=1}^{n} \bar{R}_i = 0 \tag{1}$$

The vector loop closure equation is written for dragline front-end assembly as in Equation (2).

$$\bar{R}_1 + \bar{R}_2 + \bar{R}_3 + \bar{R}_4 - \bar{R}_5 - \bar{R}_6 = 0 \tag{2}$$

Vector $\bar{R}_i$ ($i = 1,\ldots,6$) represents link i in 2-D space as a function of its scalar magnitude (r_i) in *metres* and the orientation from the sx-axis (θ) in *degrees*. The position equations are formed in x and y directions as in Equations (3) and (4).

$$r_1 c\theta_1 + r_2 c\theta_2 + r_3 c\left(\theta_4 + \frac{\pi}{2}\right) + r_4 c\theta_4 - r_5 c\theta_5 - r_6 c\theta_6 = 0 \tag{3}$$

$$r_1 s\theta_1 + r_2 s\theta_2 + r_3 s\left(\theta_4 + \frac{\pi}{2}\right) + r_4 s\theta_4 - r_5 s\theta_5 - r_6 s\theta_6 = 0 \tag{4}$$

In Equations (3) and (4) linear displacements are represented by r_i and angular displacements are represented by θ_i for all links. After obtaining position equations, velocity equations are obtained by taking the first derivative of the displacement

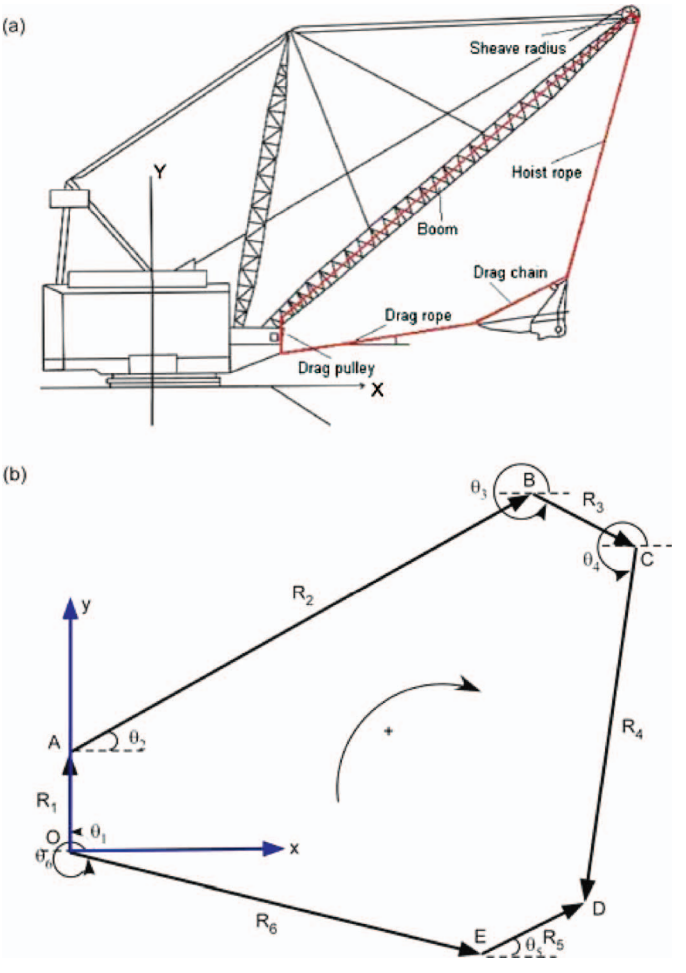

Figure 1. Dragline kinematics: (a) dragline front end assembly, (b) vector loop representation.

equations with respect to time and can be expressed in terms of a matrix format as in Equation (5).

$$\begin{bmatrix} -r_3c\theta_4 - r_4s\theta_4 & r_6s\theta_6 \\ -r_3s\theta_4 + r_4c\theta_4 & -r_6c\theta_6 \end{bmatrix} \times \begin{bmatrix} \omega_4 \\ \omega_6 \end{bmatrix} = \begin{bmatrix} -\dot{r}_4c\theta_4 + \dot{r}_5c\theta_5 - r_5s\theta_5\omega_5 + \dot{r}_6c\theta_6 \\ -\dot{r}_4s\theta_4 + \dot{r}_5s\theta_5 + r_5c\theta_5\omega_5 + \dot{r}_6s\theta_6 \end{bmatrix} \quad (5)$$

In Equation (5) $\dot{r}_i$ represents the linear velocity of the link i and ω_4 and ω_6 represent angular velocities of the hoist and drag ropes respectively. Similarly acceleration vectors are obtained by taking the second derivative of the position equations with respect to time as in Equation (6).

$$\begin{bmatrix} -r_3c\theta_4 - r_4s\theta_4 & r_6s\theta_6 \\ -r_3s\theta_4 + r_4c\theta_4 & -r_6c\theta_6 \end{bmatrix} \times \begin{bmatrix} \alpha_4 \\ \alpha_6 \end{bmatrix}$$
$$= \begin{bmatrix} -r_3s\theta_4\omega_4^2 - \ddot{r}_4c\theta_4 + 2\dot{r}_4s\theta_4\omega_4 + r_4c\theta_4\omega_4^2 + \ddot{r}_5c\theta_5 - 2\dot{r}_5s\theta_5\omega_5 \\ -\ r_5c\theta_5\omega_5^2 - r_5s\theta_5\alpha_5 + \ddot{r}_6c\theta_6 - 2\dot{r}_6s\theta_6\omega_6 - r_6c\theta_6\omega_6^2, \\ r_3c\theta_4\omega_4^2 - \ddot{r}_4s\theta_4 - 2\dot{r}_4c\theta_4\omega_4 + r_4s\theta_4\omega_4^2 + \ddot{r}_5s\theta_5 + 2\dot{r}_5c\theta_5\omega_5 \\ -\ r_5s\theta_5\omega_5^2 + r_5c\theta_5\alpha_5 + \ddot{r}_6s\theta_6 + 2r_6c\theta_6\omega_6 - r_6s\theta_6\omega_6^2 \end{bmatrix} \quad (6)$$

The reason for choosing the angular velocities and accelerations of hoist and drag ropes respectively as state variables is that the operation of dragline stripping is mostly controlled by the drag and hoist ropes.

3.2. *Dynamic modelling*

Draglines operate in a dynamic environment that leads to variable loads and forces on the machine components, and thus, the knowledge of dragline dynamics should provide enough information to make appropriate predictions of the outcome of any achievable operating cycle. The dynamic forces that arise due to accelerating inertia in the mechanism are computed for characterising the dynamic performance of the machine.

Focus areas of the dragline front-end dynamic model and analysis include the boom, the drag and hoist ropes and the rigging mechanism. Simultaneous constraint method is used for the dynamic modelling in this study. For the purpose of dynamics, it is important that the frame of reference be an inertial reference frame. In this study the inertial frame is fixed to the machine to allow the measurement of displacement, velocity and acceleration of machinery equipment.

The kinematics model equations form the foundation of the dynamic model. Next, the accelerations of the link centres of mass information are generated by using an approach similar to the vector loop. The resultant force/acceleration relationships are combined with the acceleration relationships that reflect the constraints of the mechanism. Finally, all equations are assembled into a sparse matrix in a more compact form that is solved within MATLAB and SIMULINK as part of full dynamic simulation of the mechanism.

3.2.1. *Force equations*

Force equations are obtained by applying the general form of Newton-Euler equations to each individual link as illustrated in Figure 2 to relate the forces on each link to its individual acceleration. The generalised set of Newton's Second Law equations is given in Equation (7).

$$\begin{cases} \sum_i^n F_{i,x} = M_i A_{ci,x} \\ \sum_i^n F_{i,y} = M_i A_{ci,y} \\ \sum_{i=1}^n \tau_i = I_i \alpha_i \end{cases} \quad (7)$$

It states that the acceleration of an object, produced by a net force, is directly proportional to the magnitude of the net force, in the same direction as the net force.

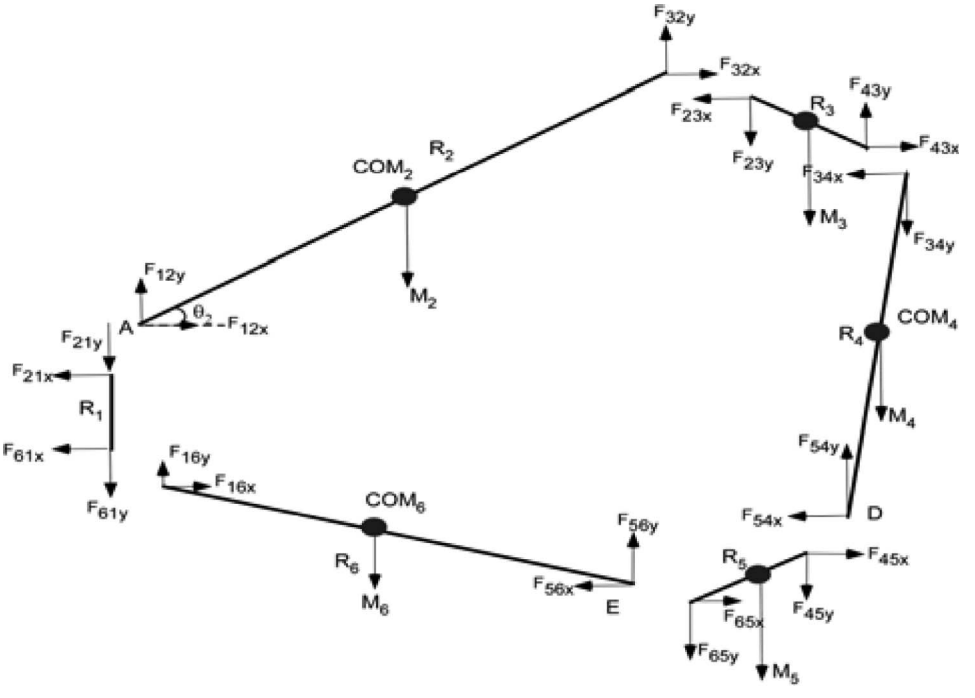

Figure 2. Free body diagrams of front-end components.

It should be noted that I_i is the moment of inertia about centre of mass (COM) of the link. Often the moment is known with respect to different axis. If that is the case, then the parallel axis theorem is applied to compute the appropriate value as in Equation (8).

$$I_{i,\text{new}} = I_i + M_i d^2 \tag{8}$$

The dynamic and static links are determined first prior to generating the force equations on each link. In that case the boom attachment point to the machine house (link R_1), the boom (link R_2) and the pulley diameter (link R_3) are fixed parts of the dragline front-end. Therefore, static limit equilibrium force equations are applied to these links. However, links R_4, R_5 and R_6 are dynamic parts and the accelerations of their centres of mass should be determined as a basis for developing the force equations. The relationship between mass and weight of each part is established by the characteristic gravitational acceleration, which has a magnitude g and is directed toward the centre of the earth. The weights, M_i ($i = 1$ to n) are vector quantities that are related to their respective masses and the gravitational acceleration by $M = mg$.

3.2.2. *Centre of mass equations*

Since the positions of the front-end components are varying during its motion, it should be noted that the COM and acceleration of COM variables also change depending on the machine kinematics. Application of Newton–Euler equations to

model the various forces on link i requires the equations for the COM accelerations. These equations relate the kinematics state of the mechanism (link displacement, velocity and accelerations) with the acceleration components of the centres of mass of the links, which are required in the force equations. In general, those accelerations that do not appear in the vector loop equation must be derived and will relate the acceleration of COM of each link to the other motion variables. The components' COM accelerations are derived for the links that have masses, such as the hoist rope (R_4), rigging (R_5) and the drag rope (R_6). To derive the COM acceleration equations of the two links, a vector relationship could be derived by inspection as in Equation (9).

$$\begin{cases} A_{c2} = \ddot{R}_{c2} \\ A_{c3} = \ddot{R}_2 + \ddot{R}_{c3} \end{cases} \tag{9}$$

In Equation (9), A_{c2} is the acceleration of the COM of link 2. To generate a link's COM acceleration, a vector relationship is utilised in which the vector sum of the previous links and the distance to the COM of the link information are summed with its corresponding second derivative generated for use in subsequent analysis. The general forms of COM accelerations of dragline front-end components in x and y directions are generated for each link in the dragline front-end mechanism. The main components of the COM acceleration equation is the distance between the end of the link and the centre of its mass, angular position from the horizontal axis, angular velocity and angular acceleration of the link.

3.2.3. Formation cutting resistance model

The force required to insert a tool into a formation is of major interest for the design and automation of earthmoving machinery [15]. The dragline bucket is attached to the front-end by a rigging mechanism and the tension forces along the drag and hoist ropes are directly related to dynamic forces acting on the bucket. Therefore, the knowledge of dragline bucket forces in excavation operation is necessary to develop the dynamic model of the dragline front-end assembly. The discrete element method (DEM) technique explicitly models the dynamic motion and mechanical interaction of each particle (body) throughout simulation. It also provides a detailed description of the positions, velocities and forces acting on each particle at discrete points in time during the analysis. The formation cutting resistance model is developed by using the mechanical relationships among soil–soil interactions and soil-tool (bucket teeth) interactions. Since time-dependent behaviour can be modelled by spring-dashpot model, it is used in the simulations. Two basic parameters, namely stiffness and damping ratio, are essential using the spring-dashpot model. The collision force model by Cleary [16] is adopted in modelling this process. In this study, the soil is defined as the assembly of 2-D circular elements. Soil particles are modelled as mono-size circular discs kinematics parameters, which change through the digging process simulation as time in Figure 3.

3.3. Model validation

To validate the model, error check analysis has been performed. For this purpose, a new function is introduced in a vector sense as shown in Equation (10) that takes the

displacement variables as input and returns a value that represents the error inherent in the computation.

$$\bar{E} = \bar{R}_1 + \bar{R}_2 + \bar{R}_3 + \bar{R}_4 - \bar{R}_5 - \bar{R}_6 \tag{10}$$

The norm of $\bar{E}$ is a scalar that indicates the absolute error in the loop closure. In this study, the acceptance tolerance limit chosen as $10 \times$ E–6, and error check is done within that tolerance for two reasons. First, the units of the front-end components and the possible error are in metres. The selected error tolerance is equivalent to a micrometre, which is negligibly small when the typical dragline size is considered. Second, it is not applicable to measure distances precisely after three decimal points. The resulting error, while increasing steadily over time due to the high-order terms in Taylor Series expansion, starts at exactly zero, which indicated that the initial conditions were well posed and never achieved a value greater than $10 \times$ E–6 m through the course of the simulation time as shown in Figure 4.

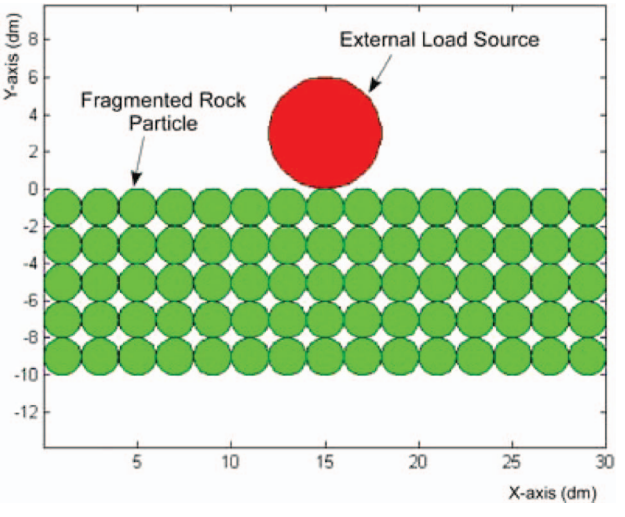

Figure 3. Rectangular clusters of circular discs.

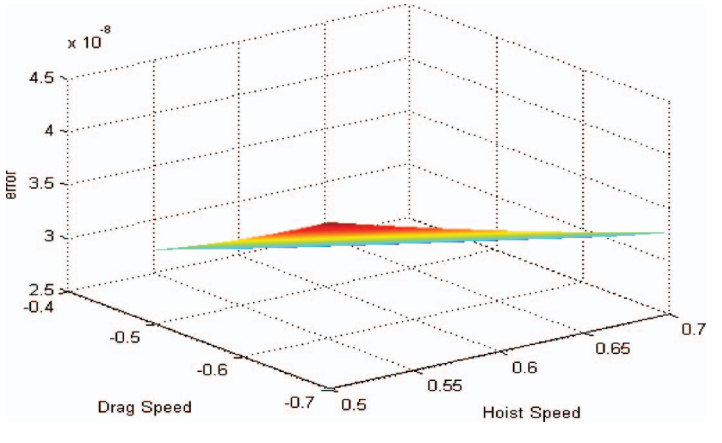

Figure 4. Truncation error through simulation time.

4. Numerical solution environment

The models developed results in a set of differential algebraic equations (DAEs), which are time-dependent, second-order ordinary differential equations (ODEs) in the form of a set of linear algebraic equations. The solution procedure followed two steps. At first, the values of the time-dependent variables were obtained from an ODE solver. The values of the time-dependent variables are used to solve the linear system concurrently with the ODE solver, which is Runge–Kutta (4,5) [17] embedded algorithm with automatic step-size control in MATLAB, at each iteration step. The linear equation system was solved using Gaussian elimination with partial pivoting. The numerical accuracy or truncation errors and stability issues have been properly assessed to ensure accurate solutions. The simulation models have been built using block modelling in MATLAB 7.0 and SIMULINK 6.0 [18]. Essentially the algorithm combines linear solver, numerical integration, simulation and analysis of the kinematic and dynamic model equations over time.

5. Simulation results

The simulation is initiated by defining the dragline model (Figure 5) and passing the input data from user-written script file. The input file contains information that characterises the dragline 3-D geometry. Then the SIMULINK block model is called by a command defined in function and then the results are post-processed and plotted on the relevant graphs. The post-processor script provides a platform for visualising the obtained results on relevant graphs, which include kinematics parameters, simulation error through experimentation time and forces.

The numerical experimentations are carried out for the MARION 7620 dragline, which has a bucket capacity of 15–27 m^3, a boom length of 91.4 m and a boom angle of 32°. A Dell Precision 670 dual processor desktop computer with a 3.0 GHz Intel Pentium 4 (Hyper-Threaded) central processing unit is used for numerical experimentation. An important aspect of a kinematics simulation is the appropriate assignment of initial conditions to the integrators. Typically, this requires that the position and velocity problem be solved by hand for at least one position of the mechanics. Table 1 contains the selected initial conditions for the model. The initial conditions are selected to ensure machine stability, optimum muck pile engagement, and motion control.

From the detailed simulation experimentation and analysis of results from the kinematics models, it was found out that there is a negative correlation between the linear displacement of the drag and hoist ropes. However, the angular displacement and velocity of the drag and hoist ropes are positively correlated. The linear change in both drag and hoist ropes are 0.85 m/sec and 0.75 m/sec, respectively.

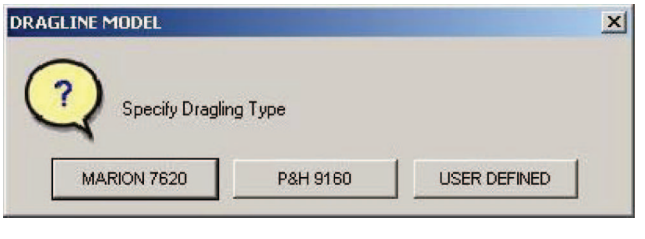

Figure 5. MATLAB GUI for dragline definitions in the main program.

Angular accelerations of both the drag and hoist ropes are close to zero and remains constant throughout the simulation (α_4: 1.06×10 E–3 $\leq \alpha_4$ 1.08×10 E–3 and α_6: -0.75×10 E–3 $\leq \alpha_6 \leq -1.3 \times 10$ E–3) as depicted in Figure 6.

While the linear velocity of the drag rope increases in a negative direction, the linear velocity of the hoist rope increases in a positive direction. The results also showed that high drag rope speed leads to low bucket filling time and vice versa.

As the resistive force acting on the bucket is a function of the bucket position into the formation, it is essential to incorporate the bucket trajectory. The bucket trajectory is obtained using the bucket kinematics as illustrated in Figure 7.

Both drag and hoist speeds have an impact on angular acceleration of the hoist rope, which copes primarily with bending on rope drums, points sheaves, deflections sheaves, and the tension force imposed by the bucket and its load [19]. Figure 8 represents the angular acceleration of the hoist rope with respect to the given initial values of drag and hoist speeds.

Important engineering data related to machine dynamics could be economically determined at a faster rate by simulating reality with a virtual prototype of a physical system. Simulation results of a dynamic model revealed that the maximum drag

Table 1. Initial conditions chosen for simulation.

Operating parameters	Symbol	Initial value
Hoist rope speed	$\dot{r}_4$	0.5–0.7 (m/sec)
Drag rope speed	$\dot{r}_6$	−0.7–0.5 (m/sec)
Linear hoist acceleration	$\ddot{r}_4$	0.01 (m/sec^2)
Linear drag chain acceleration	$\ddot{r}_5$	0 (m/sec^2)
Linear drag acceleration	$\ddot{r}_6$	−0.03 (m/sec^2)
Angular drag chain acceleration	α_5	0.05 (rad/sec^2)

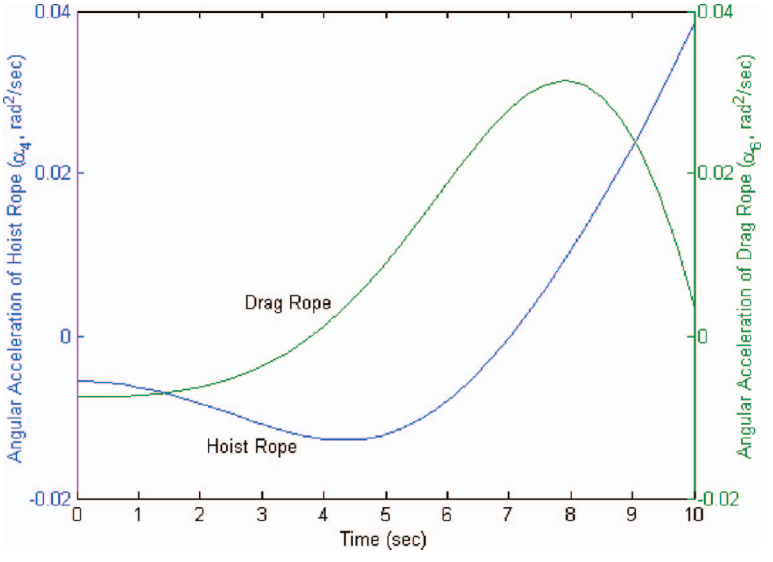

Figure 6. Angular acceleration of hoist rope (α_4) and drag rope (α_6) vs. time.

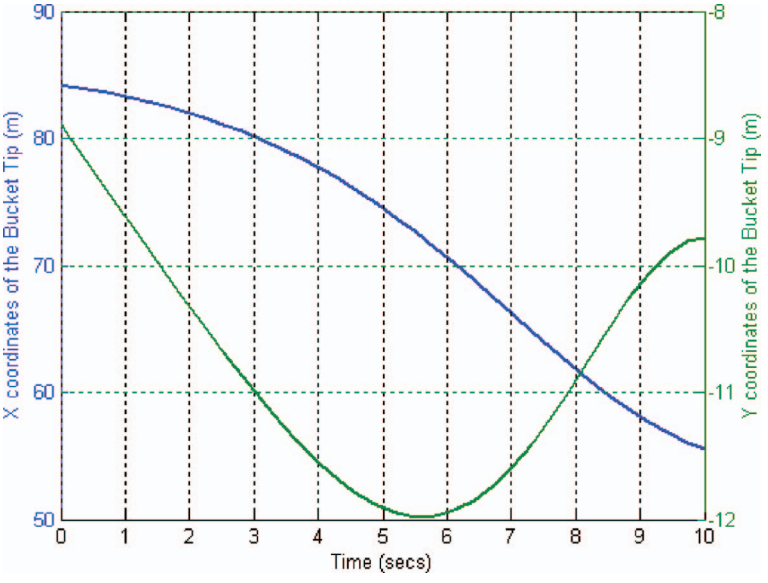

Figure 7. Bucket trajectory into formation.

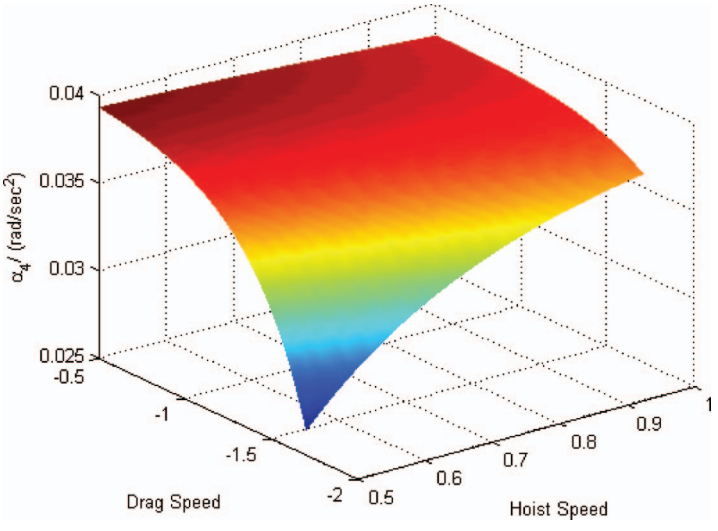

Figure 8. Angular acceleration of hoist rope (α_4), hoist and drag rope velocities ($\dot{r}_4$ and $\dot{r}_6$) vs. time.

force, which is approximately 200 kN, occurs in a simulation time of 20 sec. It is also important to note that the tension along the hoist rope is sensitive to the weight of the material in the bucket. The maximum hoist force, which is approximately 75 kN, occurs in a simulation time of 15 sec at which the bucket is filled completely. Also, the higher weight of the bucket leads to a higher initial force between the tool and the material.

The research findings showed that the maximum cutting resistant force, which is approximately 100 kN, occurs when the bucket teeth are fully engaged with the formation in a simulation time of 2.5 sec. The cutting resistant force decreases with simulation time because the cutting tool-particle collision force decreases with simulation time as shown in Figure 9. At the beginning of the simulation, the cutting resistance force is close to zero because there is no contact at the teeth of the dragline bucket. The cutting resistant force decreases with simulation time because the cutting tool-particle collision force decreases with simulation time.

The solution to the bucket rigging dynamics was obtained after generating the cutting resistance force. Figure 10 shows the solutions to the bucket rigging dynamic problem. In these results, the COM for components is assumed to be located at half of the length of the component. The drag and hoist rope forces increase and decrease through simulation time.

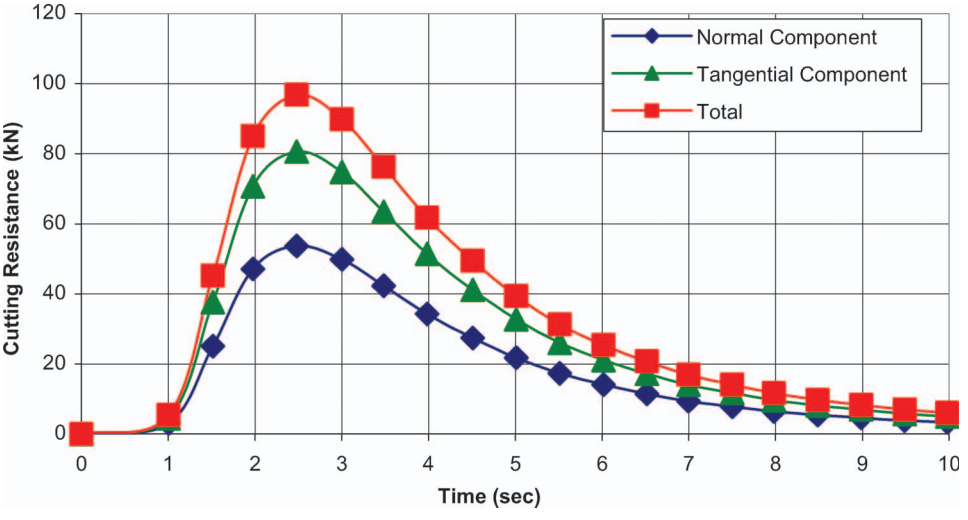

Figure 9. Cutting resistance force.

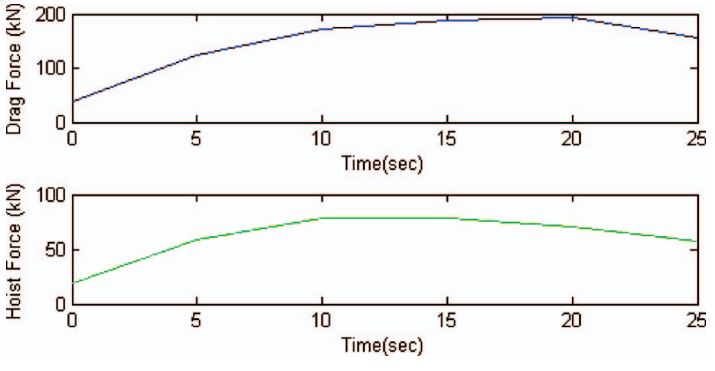

Figure 10. Bucket rigging dynamics for drag and hoist.

Since the numerical kinematics and dynamic models were developed for the 2-D dragline front-end assembly, the dynamics modelling results illustrate force generated during the planar motion of the dragline front-end. The drag force is a function of bucket displacement, cutting resistant force, and the material weight in the bucket. The maximum drag force, which is approximately 200 kN, occurs in a simulation time of 20 sec. According to motor characteristics, increasing the drag force decreases the drag velocity [20]. This was confirmed by the results obtained from drag rope kinematics simulation results, which shows the decrease in the linear velocity of the drag rope through simulation time.

In Figure 10, the change in the hoist force is also given through simulation time. Since the formation digging process is mostly governed by the drag rope, the hoist rope force can be considered as a function of the material weight in the bucket. The maximum hoist force, which is approximately 75 kN, occurs in a simulation time of 15 sec. Since the hoist rope is a connection between the suspended load and the dragline boom, the hoist force is critical parameter in determining the stress loading on the dragline boom. Therefore, the change in the bucket payload and the linear and angular acceleration of the hoist rope affect the results significantly.

The force distribution on each dragline front-end component was also simulated to understand its load distribution. Figure 11 shows the MARION 7620 dragline boom dynamics during the excavation. The results showed that the forces exerted on the boom sheave are compressive forces and the forces exerted on the boom foot are tensile forces. Since the swing motion is not included in the study, the swing torque on the boom structure is eliminated from the calculations.

The result showed that the weight of the boom is the biggest force component in the dynamics of the boom and it is critical for determining the stress loading of the boom. The vertical and horizontal force components (F_{12x} and F_{12y}) at the boom foot are the forces required to connect the body of the boom to the machine house. Therefore, estimating these forces is critical for the welding process. On the other hand, the vertical and horizontal force components (F_{32x} and F_{32y}) at the boom sheave are the forces applied to the boom sheave and they are critical for stress loading.

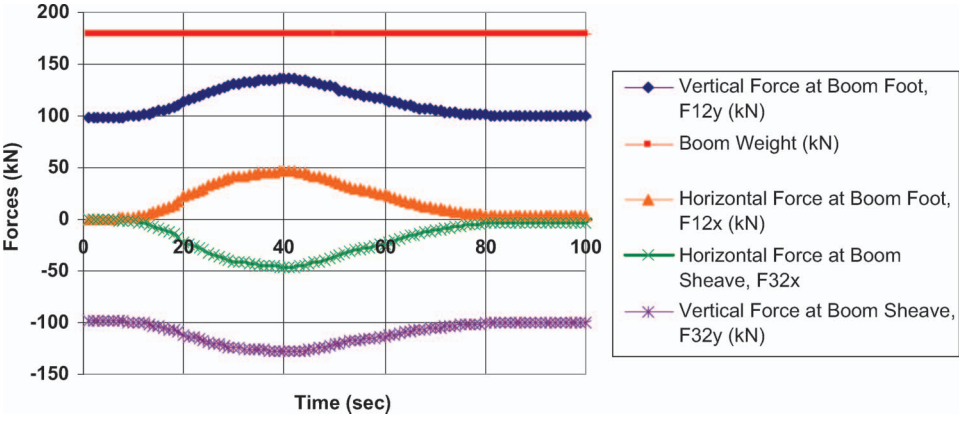

Figure 11. Boom dynamic forces.

Figure 12 shows the results of the hoist rope dynamics. The maximum hoist tension is found to be 45 kN which takes place close to the boom sheave. The results showed that the maximum tension along the hoist rope occurs when the bucket is fully loaded due to the gravitational force and accelerating inertia of the bucket and its payload. The vertical and horizontal force components (F_{34x} and F_{34y}) are the forces on the hoist rope at the pulley. Estimating these forces is significant in estimating the required rope strength and required safety factor of the rope. Knowledge of these forces provides further insight into the appropriate rope strand selection. On the other hand, the vertical and horizontal force components (F_{54x} and F_{54y}) are the forces applied at the connection point of the rope to the bucket rigging mechanism, which is subject to oscillation during the operation.

Figure 13 shows the drag rope forces as functions of the bucket and rigging kinematics and formation cutting resistant force. The vertical component of the drag

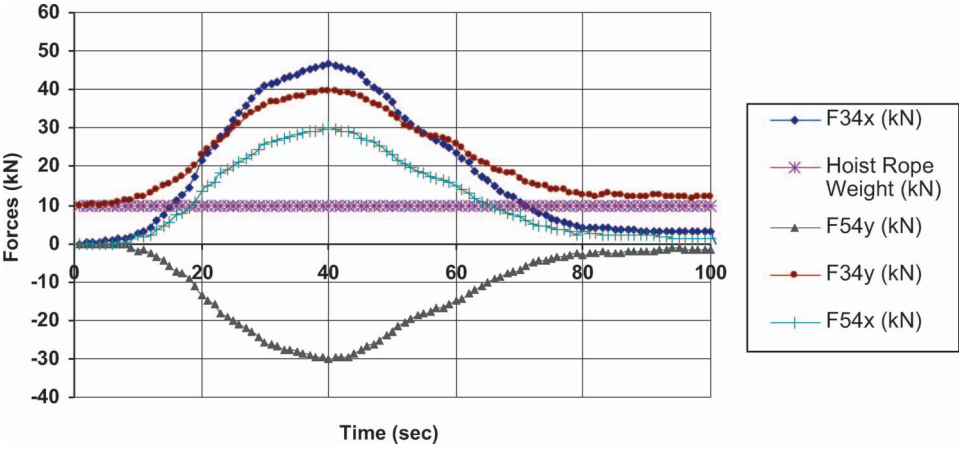

Figure 12. Hoist rope dynamics.

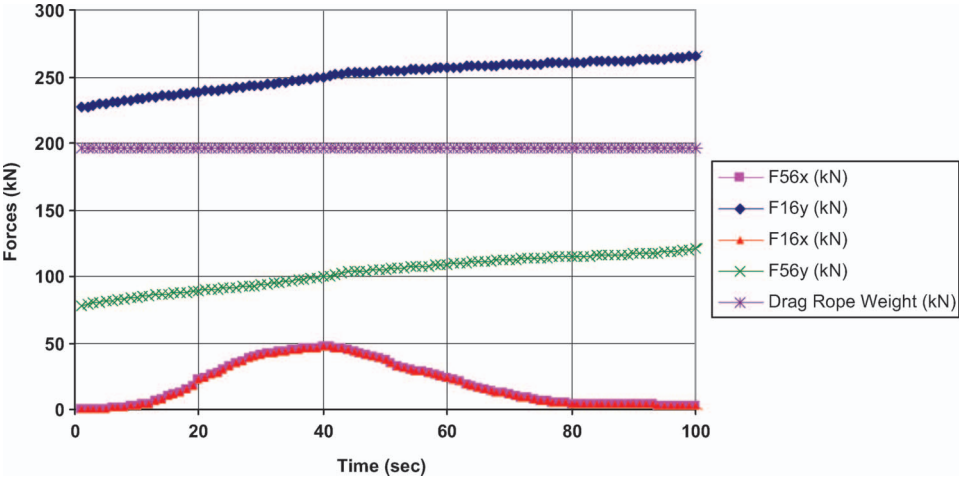

Figure 13. Drag rope dynamics.

rope tension increases continuously through the simulation time because the material inside the bucket increases within the same time period. The drag rope is constantly under the effect of tension forces in Figure 13.

In actual operating conditions, the usual practice for preventing the drag rope wear is to keep the drag rope always tight enough to prevent severe drag rope-ground interaction. Otherwise, the drag ropes are exposed to severe abrasion, especially at the pit crest, rope deformation, and inside breaking [19]. The horizontal components of the drag rope tension increase until the digging process is completed; after the bucket is filled, the horizontal tension decreases.

6. Conclusions

This research study advances a pioneering effort in dragline front-end simulation incorporating tool-formation interaction for efficient excavation. It contributed to the existing knowledge and advanced the research frontiers in dragline kinematics modelling and dynamic simulation.

This research study combines the use of an analytical literature review, kinematics and dynamic modelling, computer simulation, and detailed analysis of simulation results to achieve the research objectives. Numerical and computational techniques provided detailed information on all links and joints concerning the translational and rotational motion, displacement, velocity, and acceleration, as well as, forces, torques, and bending moments associated with these forces.

From detailed simulation experimentation and analysis of results from the kinematics models, the following conclusions have been drawn: the vector loop methodology is a useful approach to derive kinematics relationships among the different components of the mechanical system having a closed loop structure. The maximum closure error was found to be about 4×10 E–8, which is less than the required tolerance of 1×10 E–6. The simulation results showed that there is a negative correlation between the kinematics properties of hoist and drag ropes. While the angular displacement of the hoist rope increases, that of the drag rope decreases. Similarly, if the angular velocity of the hoist rope increases, then the velocity of the drag rope decreases with the same nonlinear characteristics. Also, for the same simulation time, angular acceleration of the hoist rope increases, however, the angular acceleration of the drag rope decreases.

The dynamic modelling results provided the forces exerted on the main dragline front-end components during a simulated digging operation. The research findings illustrated that the operating speed and operator performance impact the machine dynamic performance significantly. The discrete element method is proved to be an efficient tool to explicitly describe the dynamics of assemblies of particles and the mechanical interaction processes between the soil particles and the dragline bucket teeth.

On the basis of these pioneering initiatives, the results are expected to provide a solid basis for developing appropriate simulation technologies for efficient and economic dragline operations. Virtual simulation can optimise productivity by finding an optimised set of parameters for a particular dragline, which could take months to complete with physical simulations. The results could also be used for appropriate safety requirements and to provide guidelines for increasing machine reliability and maintainability for longevity and efficiency. Advances in dragline

boom stress–strain, suspension monitoring and fatigue analysis will decrease operating and maintenance costs with significant benefits to industry.

7. Recommendations

Although this research study has made a significant contribution to efficient dragline excavation, its longevity and productivity, several areas require improvements through further research. The following areas are suggested for further research investigations.

Three-dimensional kinematics and dynamic models for generating a set of optimised 3-D dragline geometries for design and operation could significantly improve and add to the body of knowledge in this research area. The research findings could be used as a basis to yield an optimised set of 3-D geometry for dragline selection and operations in random multivariable fields through factorial experimental design and experimentation.

The experiments should be designed to provide knowledge on (i) an optimised set of dragline parameters; (ii) effective and efficient interactions with the formation and (iii) minimised dragline boom stress and suspension during the operation to achieve maximum utilisation.

The results could be used to provide solutions to important dragline problems such as component vibration and boom suspension. During the swing motion, the bucket is not limited within the vertical boom plane. It can experience out-of-plane oscillations caused by the swing acceleration. Therefore, the mechanics of this bucket oscillation must be incorporated into the dragline dynamics for more realistic and more accurate results. The dragline kinematics and dynamic characteristics could be monitored by using onboard instrumentation to provide real-time data to calibrate and to verify the theoretical models.

Acknowledgement

The authors kindly acknowledge the financial support provided by the Robert H. Quenon Endowment Fund, USA and the Natural Sciences and Engineering Research Council (NSERC), Canada.

References

[1] P.G. Townson, D.N.P. Murthy, and H. Gurgenci, *Optimization of dragline load*, in *Case Studies in Reliability and Maintenance*, in *Wiley Series in Probability and Statistics*, W.R. Blischke, and D.N. Prabhakar Murthy, eds., Wiley, New Jersey, USA, 2003, pp. 517–544.

[2] P. Westcott, *Dragline and/or truck/shovel assist: some technical and business considerations*, Inaugural UNSW/Mitsubishi Lecture Notes, 2004. http://www.mining.unsw.edu.au/pdf/ MitsubishiLect_Notes_2004.pdf (Last Accessed November 21, 2006).

[3] P.D. Lawrence, F. Sassani, B. Sauder, N. Sepehri, U. Wallersteiner, and J. Wilson, *Computer-assisted control of excavator-based machines*, SAE off Highway Exposition, Milwaukee, Wisconsin, USA, SAE Technical Paper No. 932486, 1993.

[4] E. Papadulos and S. Sarkar, *On the dynamic modeling of an articulated electrohydraulic forestry machine*. Proceedings of the 1996 AIAA Forum on Advanced Developments in Space Robotics, Madison, WI, August 1–2, 1996.

[5] D.M. Bullock, S. Apte, and I.J. Oppenhim, *Force and geometry constraints in robot excavation, Space 90: Engineering Constructions and Operations in Space*, NY, 1990.

[6] L.E. Bernold, *Experimental studies on mechanics of lunar excavation*, J. Aeropsace Eng., ASCE, 4 (1991), pp. 9–22.

[7] M. Khoshzaban, F. Sassani, and P.D. Lawrence, Autonomous kinematic calibration of industrial hydraulic manipulators. *Fourth International Symposium on Robotics and Manufacturing, The American Society of Mechanical Engineers*, Santa Fe, USA, 1992, pp. 577–584.
[8] M.R. Hansen, *An automated procedure for dimensional synthesis of mechanisms*, Struct. Optimization, 5 (1993), pp. 145–151.
[9] D.K. Haneman, H. Hayes, and G.I. Lumley, *Dragline performance evaluations for tarong coal using physical modeling*. Third Large Open Pit Mining Conference, The Australian Institute of Mining and Metallurgy, Mackay, Australia, 1992, pp. 93–99.
[10] A.J. Koivo, *Kinematics of excavators (Backhoes) for transferring surface material*, J. Aerospace Eng., © American Society of Civil Engineering (ASCE), 7 (1994), pp. 17–32.
[11] S. Frimpong and Y. Hu, Hydraulic shovel simulator in surface mining excavation engineering. *12th MPES*, Kalgoorlie, West Australia, 2003.
[12] S. Frimpong and Z. Chang, KANEXP03 cable shovel dynamics and PID control scheme for efficient surface mining excavation. *SME Mining Engineering*, © SME, Littleton, CO, 2004.
[13] N. Shi and T.G. Joseph, *A New Canadian shovel dipper design for improved performance*. Proceedings of CIM Conference, Edmonton, AB, Canada, 2004.
[14] K. Awuah-Offei, S. Frimpong, and H. Askari-Nasab, Dynamic simulation of cable shovel specific energy in oil sands excavation. *Computer Applications in the Minerals Industry (CAMI 2005)*, Banff, Alberta.
[15] S. Blouin, A. Hemami, and M. Lipsett, *Review of resistive force models for earthmoving process*, J. Aerospace Eng. 14 (2001), pp. 102–110. (American Society of Civil Engineers, New York, NY, USA).
[16] P.W. Cleary, *The filling of dragline buckets*, Math. Eng. Ind. 7 (1998), pp. 1–24.
[17] J.R. Dormand and P.J. Prince, *A family of embedded Runge–Kutta formulae*, J. Computat Appl Mathematics (Elsevier B. V., Oxford, UK), 6 (1980), pp. 19–26.
[18] MATLAB 7.0 User's Guide, 2004. *The Language of Technical Computing*, © The MathWorks Inc., 24 Prime Park Way, Natick, MA 01760.
[19] T.S. Golosinski, *Performance of dragline hoist and drag ropes*, Mining Eng. 46 (1994), pp. 1285–1288.
[20] ACARP, *Modeling dragline bucket dynamics and digging (including bucket filling and animations)*, Australian Coal Association Research Program (ACARP) Research Project C3048, Final Report, January, Earth Technology Pty. Ltd., 1999, 153 pp.